

Pattern formation of parasite-host model induced by fear effectYong Ye,¹ Yi Zhao,^{1, a)} and Jiaying Zhou¹*School of Science, Harbin Institute of Technology (Shenzhen), Shenzhen 518055, China*

(Dated: 19 May 2022)

In this paper, based on the epidemiological microparasite model, a parasite-host model is established by considering the fear effect of susceptible individuals on infectors. We explored the pattern formation with the help of numerical simulation, and analyzed the effects of fear effect, infected host mortality, population diffusion rate and reducing reproduction ability of infected hosts on population activities in different degrees. Theoretically, we give the general conditions for the stability of the model under non-diffusion and considering the Turing instability caused by diffusion. Our results indicate how fear affects the distribution of the uninfected and infected hosts in the habitat and quantify the influence of the fear factor on the spatiotemporal pattern of the population. In addition, we analyze the influence of natural death rate, reproduction ability of infected hosts, and diffusion level of uninfected (infected) hosts on the spatiotemporal pattern, respectively. The results present that the growth of pattern induced by intensified fear effect follows the certain rule: cold spots \rightarrow cold spots-stripes \rightarrow cold stripes \rightarrow hot stripes \rightarrow hot spots-stripes \rightarrow hot spots. Interestingly, the natural mortality and fear effect take the opposite effect on the growth order of the pattern. From the perspective of biological significance, we find that the degree of fear effect can reshape the distribution of population to meet the previous rule.

^{a)}Electronic mail: zhao.yi@hit.edu.cn

With the development of reaction-diffusion equation, the research on the pattern formation of population model has been widely concerned. Among them, the research on spatiotemporal dynamics of predator-prey model is particularly rich. Recently, Wang et al.¹ first proposed the mathematical expression of fear effect and considered the fear effect in the traditional predator-prey model. It was found that the addition of fear effect brought complex dynamic phenomena. Since then, many predator-prey models with fear effect have been studied. Considering that the fear effect also exists between uninfected host and infected host. Therefore, this paper attempts to introduce the fear effect into the epidemiological microparasite model and construct a parasite-host model with fear effect. With the help of computer, we simulate the distribution of population under different degrees of fear, and combined with other ecological factors to explore how the distribution of population will change under the interference of various factors. Our results show that the growth of pattern satisfies some laws under different ecological factors. Hopefully, this work will provide us further understanding of population dynamics in a real environment stimulated by the fear effect.

I. INTRODUCTION

Ecologists recognize that diseases and parasites play an important role in population dynamics²⁻⁵. The spatial components of ecological interactions have been identified as an important factor in how populations operate and form. However, understanding the role of space is challenging both theoretically and empirically⁶⁻⁹. In recent years, many studies have shown that pattern formation in parasite-host model is an appropriate tool to understand the basic mechanism of parasite spatiotemporal dynamics. In 2003, Hwang and Kuang established a parasite-host ordinary differential equation (ODE) model² based on the work of Ebert et al.³. On this basis, the dynamics and pattern formation of the reaction-diffusion parasite-host model were studied in^{10,11}, the model is as follows:

$$\begin{cases} \frac{\partial S}{\partial t} - d_1 \Delta S = r(S + \rho I)(1 - a(S + I)) - \frac{\beta SI}{S+I}, & x \in \Omega, \quad t > 0, \\ \frac{\partial I}{\partial t} - d_2 \Delta I = \frac{\beta SI}{S+I} - \mu I, & x \in \Omega, \quad t > 0, \\ \frac{\partial S}{\partial \mathbf{n}} = \frac{\partial I}{\partial \mathbf{n}} = 0, & x \in \partial\Omega, \quad t > 0, \\ S(x, 0) = S_0(x), I(x, 0) = I_0(x), & x \in \Omega, \end{cases} \quad (1)$$

where $\frac{\beta SI}{S+I}$ denotes the frequency-dependent transmission^{2,10}, the variable S represents density of uninfected (susceptible) hosts, and I represents density of infected (infective) hosts. The habitat $\Omega \subset \mathbb{R}^n$ is a positive bounded region with smooth boundary $\partial\Omega$, x represents location in the habitat, \mathbf{n} stands for the outward unit normal vector on $\partial\Omega$, d_1 and d_2 respectively represent self diffusion coefficients of uninfected host and infected host, and Δ denotes Laplacian operator. In this paper we assume that the habitat is closed, which means that the infected (uninfected) host population inside the habitat cannot go out, while the infected (uninfected) host population outside the habitat cannot enter, and there is no host population on the boundary. That is to say, the boundary condition we consider is zero-flux (i.e., Neumann boundary). The biological significance of other parameters are described in Table II. It is worth noting that all parameters are positive and $0 \leq \rho \leq 1$.

In recent years, the relevant experiments on risk perception (i.e., indirect effect) of biological population have been proposed. Zanette et al.'s experiment on the perception of predation risk by songbirds shows that the number of offspring produced each year is reduced by 40% just by the perception of predation risk. So the perception of predation risk takes obviously significant effect on the dynamics of biological population¹². Abbey-Lee et al. adopts playback technology to conduct experiments on the perceived predation risk in nest-box populations of wild great tits (*Parus major*), to investigate the effects of nonconsumptive on the predation behavior, the morphology of bird predators, and the individual responses to predation¹³. Their results show that the sensitivity of individuals to predation risk leads to the different adaptability. As a typical and representative indirect effect, the fear factor is used to describe the physiological changes caused by the stress behavior of the prey population since the prey needs to be alert to predators coming at any time¹⁴. In order to characterize the influence of anti-predator behavior on predator-prey system, Wang et al. firstly propose a predator-prey model with consideration of the fear factor in the growth of the prey¹. After that, the researchers consider that the outbreak and spread of infectious diseases would bring people fear. In literature¹⁵, they think that the susceptible population has a fear effect, which shows that the fear effect can reduce the growth rate of the susceptible population. Follow-

ing their ideas, we assume that the uninfected population has anti-infected behavior, that is, the fear effect on infected population. We then consider the growth function of the uninfected population with fear effect as follows: $\frac{dS}{dt} = [F(k, I)r]S$. $F(k, I)$ accounts for the cost of anti-infected due to uninfected population, and the parameter k reflects the level of fear which drives anti-infected behavior of the uninfected host. Which is similar to^{1,16}, in Table I, we show the conditions that the fear factor $F(k, I)$ satisfies.

TABLE I. Conditions that fear factor $F(k, I)$ satisfies.

| Conditions | Statements |
|---|--|
| $F(0, I) = 1$ | When there is no fear, the maximum birth rate of uninfected population did not decrease |
| $F(k, 0) = 1$ | When there is no infected host, the maximum birth rate of uninfected population did not decrease |
| $\lim_{k \rightarrow \infty} F(k, I) = 0$ | When anti-infected behavior is large enough, the uninfected production reduces to 0 |
| $\lim_{I \rightarrow \infty} F(k, I) = 0$ | When infected population is large enough, the uninfected production reduces to 0 |
| $\frac{\partial F(k, I)}{\partial k} < 0$ | When anti-infected behavior increases, the uninfected production decreases |
| $\frac{\partial F(k, I)}{\partial I} < 0$ | When infected population increases, the uninfected production decreases |

Population dynamics and epidemic dynamics models considering fear effect have been widely studied^{14–28}. This paper focus on the influence of fear factor on the pattern formation of host parasite model and the complex dynamic changes. Following¹, we introduce the fear effect $F(k, I) := \frac{1}{1+kI}$ as the fear effect in model (1). which satisfies the conditions in Table I. Then we obtained the following model:

$$\begin{cases} \frac{\partial S}{\partial t} - d_1 \Delta S = \frac{rS}{1+kI} + r\rho I - ra(S + \rho I)(S + I) - \frac{\beta SI}{S+I}, & x \in \Omega, \quad t > 0, \\ \frac{\partial I}{\partial t} - d_2 \Delta I = \frac{\beta SI}{S+I} - \mu I, & x \in \Omega, \quad t > 0, \\ \frac{\partial S}{\partial \mathbf{n}} = \frac{\partial I}{\partial \mathbf{n}} = 0, & x \in \partial\Omega, \quad t > 0, \\ S(x, 0) = S_0(x), I(x, 0) = I_0(x), & x \in \Omega. \end{cases} \quad (2)$$

The main structure of this paper is as follows. In Section II, we discuss the existence condition of equilibrium in the non-diffusion model (2), and obtain the stability condition through the general linear stability analysis. In Section III, we analyze the diffusion model (2) and find out the Turing space where Turing instability occurs. Then, the hexagonal and stripe pattern of model (2) are studied by using amplitude equation near the critical value of control parameters. In Section IV, we use numerical simulation to illustrate the different patterns we found. Finally, the results and future work are discussed.

II. MODEL WITHOUT DIFFUSION

Since this paper mainly discusses Turing instability caused by diffusion, and the premise of Turing instability is to ensure that the positive equilibrium is stable without diffusion. We first consider the case of ODE model without diffusion, i.e., $d_1 = d_2 = 0$. Then the existence and stability conditions of nontrivial (positive) equilibria will be given.

A. Existence of Equilibria

If

$$\begin{cases} \frac{rS_{n*}}{1+kI_{n*}} + r\rho I_{n*} - ra(S_{n*} + \rho I_{n*})(S_{n*} + I_{n*}) - \frac{\beta S_{n*}I_{n*}}{S_{n*}+I_{n*}} = 0, \\ \frac{\beta S_{n*}I_{n*}}{S_{n*}+I_{n*}} - \mu I_{n*} = 0, n = (1, 2, 3). \end{cases} \quad (3)$$

Theorem 1. *Model (2) has a trivial equilibrium $E_0 = (0, 0)$ and a semi-trivial equilibrium $E_1 = (\frac{1}{a}, 0)$. Furthermore, when $B(k)^2 - 4A(k)C(k) > 0$ and $C(k) < 0$, model (2) has a positive equilibrium $E_{2*} = (S_{2*}, I_{2*})$, where $S_{2*} = \frac{-B(k) + \sqrt{B(k)^2 - 4A(k)C(k)}}{2A(k)}$, $I_{2*} = \frac{(\beta - \mu)S_{2*}}{\mu}$, ($S_{2*} > S_{3*}$, $I_{2*} > I_{3*}$); If $B(k)^2 - 4A(k)C(k) = 0$, the positive equilibrium $E_{1*} = (S_{1*}, I_{1*})$, where $S_{1*} = \frac{-B(k)}{2A(k)}$, $I_{1*} = \frac{(\beta - \mu)S_{1*}}{\mu}$ and $\beta > \mu$.*

Proof. We can calculate that model (2) has a trivial equilibrium $E_0 = (0, 0)$ and a semi-trivial equilibrium $E_1 = (\frac{1}{a}, 0)$. Furthermore, it can be obtained from Eq. (3) that

$$I_{n*} = \frac{(\beta - \mu)S_{n*}}{\mu}, \quad (4)$$

and

$$\begin{aligned} & rS_{n*}(S_{n*} + I_{n*}) + r\rho I_{n*}(S_{n*} + I_{n*})(1 + kI_{n*}) \\ & - ra(S_{n*} + \rho I_{n*})(S_{n*} + I_{n*})^2(1 + kI_{n*}) - \beta S_{n*}I_{n*}(1 + kI_{n*}) = 0, \end{aligned} \quad (5)$$

By taking Eq. (4) into Eq. (5), we can get

$$\begin{aligned} & r(1 + \frac{(\beta - \mu)}{\mu}) + r\rho \frac{(\beta - \mu)}{\mu}(1 + \frac{(\beta - \mu)}{\mu})(1 + k\frac{(\beta - \mu)S_{n*}}{\mu}) \\ & - raS_{n*}(1 + \rho \frac{(\beta - \mu)}{\mu})(1 + \frac{(\beta - \mu)}{\mu})^2(1 + k\frac{(\beta - \mu)S_{n*}}{\mu}) \\ & - \beta \frac{(\beta - \mu)}{\mu}(1 + k\frac{(\beta - \mu)S_{n*}}{\mu}) = 0, \end{aligned} \quad (6)$$

that is

$$\begin{aligned} & r(1+m) + r\rho m(1+m)(1+kmS_{n*}) \\ & - raS_{n*}(1+\rho m)(1+m)^2(1+kmS_{n*}) \\ & - \beta m(1+kmS_{n*}) = 0, \end{aligned} \quad (7)$$

where

$$m = \frac{\beta - \mu}{\mu}. \quad (8)$$

Then, we obtain

$$\begin{aligned} & kram(1+\rho m)(1+m)^2S_{n*}^2 + (k\beta m^2 + ra(1+\rho m)(1+m)^2 - kr\rho m^2(1+m))S_{n*} \\ & + \beta m - r(1+m)(1+\rho m) = 0. \end{aligned} \quad (9)$$

Let

$$A(k) = kram(1+\rho m)(1+m)^2 > 0, \quad (10)$$

$$B(k) = k\beta m^2 + ra(1+\rho m)(1+m)^2 - kr\rho m^2(1+m), \quad (11)$$

$$C(k) = \beta m - r(1+m)(1+\rho m), \quad (12)$$

that is

$$A(k)S_{n*}^2 + B(k)S_{n*} + C(k) = 0. \quad (13)$$

Eq. (13) has the following positive solutions:

$$S_{n*} = \frac{-B(k) \pm \sqrt{B(k)^2 - 4A(k)C(k)}}{2A(k)}. \quad (14)$$

We then obtain the following results:

- Let $B(k)^2 - 4A(k)C(k) < 0$, then model (2) has no positive equilibrium.
- Let $B(k)^2 - 4A(k)C(k) = 0$, when $B(k) < 0$, model (2) has a positive equilibrium $E_{1*} = (S_{1*}, I_{1*})$, where $S_{1*} = \frac{-B(k)}{2A(k)}$, $I_{1*} = \frac{(\beta - \mu)S_{1*}}{\mu}$.
- Let $B(k)^2 - 4A(k)C(k) > 0$,

1. when $B(k) < 0$ and $C(k) > 0$, model (2) has two positive equilibrium $E_{(2,3)*} = (S_{(2,3)*}, I_{(2,3)*})$, where $S_{(2,3)*} = \frac{-B(k) \pm \sqrt{B(k)^2 - 4A(k)C(k)}}{2A(k)}$, $I_{(2,3)*} = \frac{(\beta - \mu)S_{(2,3)*}}{\mu}$,

2. when $C(k) < 0$, model (2) has a positive equilibrium $E_{2*} = (S_{2*}, I_{2*})$ where $S_{2*} = \frac{-B(k) + \sqrt{B(k)^2 - 4A(k)C(k)}}{2A(k)}$, $I_{2*} = \frac{(\beta - \mu)S_{2*}}{\mu}$, ($S_{2*} > S_{3*}$, $I_{2*} > I_{3*}$),
3. when $B(k) > 0$ and $C(k) > 0$, model (2) has no positive equilibrium.

Remark 1. • When $B(k_1) = k_1\beta m^2 + ra(1 + \rho m)(1 + m)^2 - k_1r\rho m^2(1 + m) = 0$, we obtain

$$k_1 = \frac{ra(1 + \rho m)(1 + m)^2}{r\rho m^2(1 + m) - \beta m^2}.$$

- When $C(k) = \beta m - r(1 + m)(1 + \rho m) = 0$, we obtain $\beta = \frac{r(1 + \rho m)(1 + m)}{m}$.

In summary, according to Remark 1, we can find that when $C(k) = \beta m - r(1 + m)(1 + \rho m) > 0$ and $\beta > \frac{r(1 + \rho m)(1 + m)}{m}$ that is, $B(k) = k\beta m^2 + ra(1 + \rho m)(1 + m)^2 - kr\rho m^2(1 + m) > 0$. There are no two positive equilibria in the model (2). The proof of the Theorem 1 is completed. \square

B. Stability Analysis

In this subsection, we will analyze the stability of trivial equilibrium $E_0 = (0, 0)$, semi-trivial equilibrium $E_1 = (\frac{1}{a}, 0)$ and nontrivial equilibrium (positive equilibrium) $E_{n*} = (S_{n*}, I_{n*})$, ($n = 1, 2$).

Theorem 2. (1): $E_0 = (0, 0)$ is a saddle point;

(2): If $\beta < \mu$, then $E_1 = (\frac{1}{a}, 0)$ is a stable node; if $\beta > \mu$, $E_1 = (\frac{1}{a}, 0)$ is a saddle point;

(3): When Theorem 1 holds, if $\text{Det}(J_{n*}) = a_{10}b_{01} - a_{01}b_{10} > 0$, there are two conditions:

- $r(m + 1) - \beta m > 0$ and $S_{n*} > S_{n*}^+$, we can calculate $\text{Tr}(J_{n*}) = a_{10} + b_{01} < 0$, then $E_{(1,2)*} = (S_{(1,2)*}, I_{(1,2)*})$ is stable;
- $r(m + 1) - \beta m \leq 0$, we can find $\text{Tr}(J_{n*}) = a_{10} + b_{01} < 0$, then $E_{(1,2)*} = (S_{(1,2)*}, I_{(1,2)*})$ is stable.

Proof. We provide stability analysis by calculating the eigenvalues of Jacobian matrix of the model (2). Let

$$f(S, I) = \frac{rS}{1 + kI} + r\rho I - ra(S + \rho I)(S + I) - \frac{\beta SI}{S + I}, \quad (15)$$

$$g(S, I) = \frac{\beta SI}{S + I} - \mu I, \quad (16)$$

the Jacobian matrix J for model (2) is

$$J = \begin{pmatrix} \frac{\partial f}{\partial S} & \frac{\partial f}{\partial I} \\ \frac{\partial g}{\partial S} & \frac{\partial g}{\partial I} \end{pmatrix}, \quad (17)$$

where

$$\begin{aligned} \frac{\partial f}{\partial S} &= \frac{r}{1+kI} - ra(2S + (\rho + 1)I) - \frac{\beta I^2}{(S+I)^2}, \quad \frac{\partial g}{\partial S} = \frac{\beta I^2}{(S+I)^2}, \\ \frac{\partial f}{\partial I} &= -\frac{rkS}{(1+kI)^2} + r\rho - ra(2\rho I + (\rho + 1)S) - \frac{\beta S^2}{(S+I)^2}, \quad \frac{\partial g}{\partial I} = \frac{\beta S^2}{(S+I)^2} - \mu. \end{aligned}$$

Evaluating the Jacobian matrix for model (2) at $E_0 = (0, 0)$, we find

$$J_0 = \begin{pmatrix} r & r\rho \\ 0 & -\mu \end{pmatrix}, \quad (18)$$

the characteristic polynomial is

$$H_0(\lambda) = \lambda^2 - Tr(J_0)\lambda + Det(J_0), \quad (19)$$

where $Det(J_0) < 0$, so we can see the trivial equilibrium $E_0 = (0, 0)$ is a saddle point.

Given the Jacobian matrix for the model (2) evaluated at $E_1 = (\frac{1}{a}, 0)$, we find

$$J_1 = \begin{pmatrix} -r & -\frac{rk}{a} + r\rho - r(\rho + 1) - \beta \\ 0 & \beta - \mu \end{pmatrix}, \quad (20)$$

and the characteristic polynomial is

$$H_1(\lambda) = \lambda^2 - Tr(J_1)\lambda + Det(J_1), \quad (21)$$

so we can calculate if $\beta < \mu$, then $E_1 = (\frac{1}{a}, 0)$ is a stable node; if $\beta > \mu$, $E_1 = (\frac{1}{a}, 0)$ is a saddle point.

The Jacobian matrix for the model (2) evaluated at $E_{n*} = (S_{n*}, I_{n*})$, ($n = 1, 2$) is given by

$$J_{n*} = \begin{pmatrix} a_{10} & a_{01} \\ b_{10} & b_{01} \end{pmatrix}, \quad (22)$$

where

$$\begin{aligned} a_{10} &= \frac{r}{1+kI_{n*}} - ra(2S_{n*} + (\rho + 1)I_{n*}) - \frac{\beta I_{n*}^2}{(S_{n*}+I_{n*})^2}, \quad b_{10} = \frac{\beta I_{n*}^2}{(S_{n*}+I_{n*})^2}, \\ a_{01} &= -\frac{rkS_{n*}}{(1+kI_{n*})^2} + r\rho - ra(2\rho I_{n*} + (\rho + 1)S_{n*}) - \frac{\beta S_{n*}^2}{(S_{n*}+I_{n*})^2}, \quad b_{01} = \frac{\beta S_{n*}^2}{(S_{n*}+I_{n*})^2} - \mu. \end{aligned}$$

The characteristic polynomial is

$$H_{n*}(\lambda) = \lambda^2 - Tr(J_{n*})\lambda + Det(J_{n*}), \quad (23)$$

where

$$Tr(J_{n*}) = a_{10} + b_{01}, \quad Det(J_{n*}) = a_{10}b_{01} - a_{01}b_{10}, \quad (24)$$

and

$$\begin{aligned} Tr(J_{n*}) = & \frac{1}{(1+m)(1+mkS_{n*})}(-ramk(1+m)(2+m(\rho+1))S_{n*}^2 \\ & + (-\beta km^2 - ra(1+m)(2+m(\rho+1)))S_{n*} + r(m+1) - \beta m), \end{aligned} \quad (25)$$

$$\begin{aligned} Det(J_{n*}) = & \frac{(\beta - \mu)}{\beta} \left(\frac{rks(\beta - \mu)}{(1 + kI_{n*})^2} + ra(S_{n*}(\rho(\beta - \mu) + \beta + \mu) + I_{n*}(\rho(2\beta - \mu) + \mu)) \right. \\ & \left. + (\beta - \mu)\mu - \frac{r\mu}{1 + kI_{n*}} - r\rho(\beta - \mu) \right). \end{aligned} \quad (26)$$

If $Det(J_{n*}) = a_{10}b_{01} - a_{01}b_{10} < 0$, then $E_{(1,2)*} = (S_{(1,2)*}, I_{(1,2)*})$ is saddle; If $Det(J_{n*}) = a_{10}b_{01} - a_{01}b_{10} > 0$ and $Tr(J_{n*}) = a_{10} + b_{01} < 0$, then $E_{2*} = (S_{2*}, I_{2*})$ is stable, otherwise, $E_{2*} = (S_{2*}, I_{2*})$ is unstable. Next, we discuss the value sign of $Tr(J_{n*})$ respectively. First, we discuss the sign of $Tr(J_{n*}) = \frac{1}{(1+m)(1+mkS_{n*})}(-ramk(1+m)(2+m(\rho+1))S_{n*}^2 + (-\beta km^2 - ra(1+m)(2+m(\rho+1)))S_{n*} + r(m+1) - \beta m)$. From the above, we can easily know that S_{n*} is positive, $-ramk(1+m)(2+m(\rho+1)) < 0$ and $-\beta km^2 - ra(1+m)(2+m(\rho+1)) < 0$. If $r(m+1) - \beta m \leq 0$, then $Tr(J_{n*})$ must be less than 0. If $r(m+1) - \beta m > 0$, then we regard S_{n*} as the solution of $Tr(J_{n*}) = 0$. Therefore, it is easy to know that the equation $-ramk(1+m)(2+m(\rho+1))S_{n*}^2 + (-\beta km^2 - ra(1+m)(2+m(\rho+1)))S_{n*} + r(m+1) - \beta m = 0$ has two roots S_{n*}^+ , S_{n*}^- , and $S_{n*}^+ > 0 > S_{n*}^-$. Where

$$S_{n*}^+ = \frac{\beta km^2 + ra(1+m)(2+m(\rho+1)) - \sqrt{\Delta}}{-2ramk(1+m)(2+m(\rho+1))},$$

and

$$\Delta = (\beta km^2 + ra(1+m)(2+m(\rho+1)))^2 + 4(ramk(1+m)(2+m(\rho+1)))(r(m+1) - \beta m).$$

So far, we can conclude that if $S_{n*} > S_{n*}^+$, then $Tr(J_{n*}) < 0$. The proof of the theorem is completed. \square

C. Example

In this subsection, we will provide a numerical example to illustrate the case that the positive equilibrium $E_{2*} = (S_{2*}, I_{2*})$ is stable. Here, the parameters are $d_1 = d_2 = 0$, $k = 0.01$, $\mu = 0.55$,

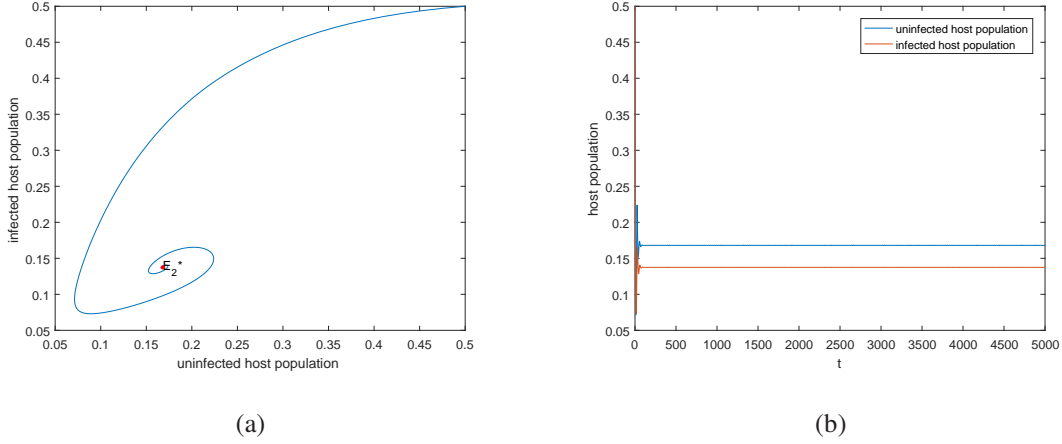


FIG. 1. Phase trajectory diagram of model (2): $E_{2*} = (0.1680, 0.1375)$ is stable

and $\rho = 0.1$ and see Table II for others. Therefore, model (2) is in the following form:

$$\begin{cases} \frac{dS}{dt} = \frac{0.6S}{1+0.01I} + 0.06I - 0.6(S+0.1I)(S+I) - \frac{SI}{S+I}, \\ \frac{dI}{dt} = \frac{SI}{S+I} - 0.55I. \end{cases} \quad (27)$$

Under this scenario, $Tr(J_{2*}) = -0.1431 < 0$ and $Det(J_{2*}) = 0.0452 > 0$. According to Theorem 2, the positive equilibrium $E_{2*} = (S_{2*}, I_{2*}) = (0.1680, 0.1375)$ is stable. The phase trajectory diagram and time series diagram of the numerical example (27) are shown in Fig. 1.

III. MODEL WITH DIFFUSION

A. Turing instability

The purpose of this subsection is to analyze the stability change caused by diffusion, i.e. Turing instability. Similar to references^{10,17,20,29–31}, the linearization form of model (2) at positive equilibrium $E_{n*} (S_{n*}, I_{n*})$ is as follows

$$\begin{aligned} \frac{\partial u}{\partial t} &= a_{10}u + a_{01}v - j^2 d_1 u, \\ \frac{\partial v}{\partial t} &= b_{10}u + b_{01}v - j^2 d_2 v, \end{aligned} \quad (28)$$

where $u = S - S_{n*}$, $v = I - I_{n*}$, and (u, v) are small perturbations around the equilibrium point $E_{n*} (S_{n*}, I_{n*})$ and have the form

$$\begin{pmatrix} u \\ v \end{pmatrix} = \begin{pmatrix} \varepsilon \exp(i\mathbf{j}\mathbf{r} + \lambda_j t) \\ \delta \exp(i\mathbf{j}\mathbf{r} + \lambda_j t) \end{pmatrix}, \quad (29)$$

where $\varepsilon \ll 1$ and $\delta \ll 1$, $j = |\mathbf{j}|$ is the wave number, \mathbf{r} is the directional vector and λ_j is the wave frequency. The characteristic equation of the linearized model (28) is given by

$$(J_{n*}^j - \lambda_j I) \begin{pmatrix} u \\ v \end{pmatrix} = 0, \quad (30)$$

where

$$J_{n*}^j = \begin{pmatrix} a_{10} - d_1 j^2 & a_{01} \\ b_{10} & b_{01} - d_2 j^2 \end{pmatrix}. \quad (31)$$

Eq. (30) can be written as

$$\lambda_j^2 - \text{Tr}(J_{n*}^j) \lambda_j + \text{Det}(J_{n*}^j) = 0, \quad (32)$$

where

$$\begin{aligned} \text{Tr}(J_{n*}^j) &= \text{Tr}(J_{n*}) - (d_1 + d_2) j^2 = a_{10} + b_{01} - (d_1 + d_2) j^2, \\ \text{Det}(J_{n*}^j) &= (a_{10} - d_1 j^2)(b_{01} - d_2 j^2) - a_{01} b_{10} \\ &= j^4 d_1 d_2 - j^2 (a_{10} d_2 + b_{01} d_1) + \det(J_{n*}), \end{aligned} \quad (33)$$

and J_{n*} is given in Eq. (22). The roots of the characteristic Eq. (31) are:

$$\lambda_j^\pm = \frac{\text{Tr}(J_{n*}^j) \pm \sqrt{(\text{Tr}(J_{n*}^j))^2 - 4 \text{Det}(J_{n*}^j)}}{2}. \quad (34)$$

When the positive equilibrium of model (2) is stable without diffusion, $\text{Tr}(J_{n*}^j)$ is negative and

$$\text{Det}(J_{n*}^j) > 0. \quad (35)$$

The diffusive model (2) will be locally asymptotically stable. We can find that the positive equilibrium is stable without diffusion ($j = 0$), but it may be unstable with diffusion ($j \neq 0$), i.e., Turing bifurcation. Obviously, $\text{Tr}(J_{n*}^j) < \text{Tr}(J_{n*}) < 0$, and therefore, the stability of positive equilibrium will change only when

$$\begin{aligned} \text{Det}(J_{n*}^j) &= (a_{10} - d_1 j^2)(b_{01} - d_2 j^2) - a_{01} b_{10} \\ &= j^4 d_1 d_2 - j^2 (a_{10} d_2 + b_{01} d_1) + \det(J_{n*}) \end{aligned} \quad (36)$$

is negative. The minimum of $\text{Det}(J_{n*}^j)$ occurs at $j^2 = j_{cr}^2$, where

$$j_{cr}^2 = \frac{a_{10} d_2 + b_{01} d_1}{2 d_1 d_2} > 0. \quad (37)$$

As $a_{10} + b_{01} < 0$, j_{cr}^2 is real and d_1, d_2 are always positive, we must have $a_{10}b_{01} < 0$. Thus, a sufficient condition for instability is $\text{Det}(j_{cr}^2) < 0$, where

$$\text{Det}(j_{cr}^2) = (a_{10}b_{01} - a_{01}b_{10}) - \frac{(a_{10}d_2 + b_{01}d_1)^2}{4d_1d_2}. \quad (38)$$

Therefore, the condition of Turing instability is as follows:

$$a_{10}d_2 + b_{01}d_1 > 2\sqrt{d_1d_2}\sqrt{a_{10}b_{01} - a_{01}b_{10}}. \quad (39)$$

Obviously, when $j^2 \in (j_-^2, j_+^2)$, $\text{Det}(j_{cr}^2) < 0$, where

$$j_{\pm}^2 = \frac{(a_{10}d_2 + b_{01}d_1) \pm \sqrt{(a_{10}d_2 + b_{01}d_1)^2 - 4d_1d_2\text{Det}(j_{cr}^2)}}{2d_1d_2}. \quad (40)$$

B. Weakly nonlinear analysis

It is pointed out that the amplitude equation is usually used to describe the evolution of dynamical system near bifurcation, showing a critical slowing down³². Note that when the control parameters are close to the threshold of Turing bifurcation, the eigenvalues related to critical modes are close to zero, that is, the critical mode is slow mode, then the whole dynamics can be attributed to the dynamic of active slow mode^{20,29,30,33,34}. In this section, we will use the standard multiscale analysis to deduce the amplitude equation. We rewrite the transformed form of model (2) at the positive spatially homogeneous steady state $E_{n*}(S_{2*}, I_{2*})$ as follows and denote by $(U, V)^T$ the perturbation solution $(U - S_{2*}, V - I_{2*})^T$ of model (2).

$$\frac{\partial X}{\partial t} = LX + \mathbf{H}, \quad (41)$$

where $X = (U, V)^T$. The linear operator L can be defined as:

$$L = \begin{pmatrix} a_{10} + d_1\Delta & a_{01} \\ b_{10} & b_{01} + d_2\Delta \end{pmatrix}, \quad (42)$$

and \mathbf{H} be given by

$$\mathbf{H} = \begin{pmatrix} a_{20}U^2 + a_{11}UV + a_{02}V^2 + a_{30}U^3 + a_{21}U^2V + a_{12}UV^2 + a_{03}V^3 + o(\varepsilon^3) \\ b_{20}U^2 + b_{11}UV + b_{02}V^2 + b_{30}U^3 + b_{21}U^2V + b_{12}UV^2 + b_{03}V^3 + o(\varepsilon^3) \end{pmatrix}, \quad (43)$$

where

$$a_{20} = -ra + \frac{\beta I_{2*}^2}{(S_{2*} + I_{2*})^3}, a_{11} = -ra(\rho + 1) - \frac{2\beta S_{2*}I_{2*}}{(S_{2*} + I_{2*})^3} - \frac{rk}{(1 + kI_{2*})^2},$$

Pattern formation of parasite-host model induced by fear effect

$$\begin{aligned}
a_{02} &= \frac{rk^2 S_{2*}}{(1+kl_{2*})^3} - rap - \frac{\beta S_{2*} I_{2*}}{(S_{2*}+I_{2*})^3}, \quad b_{20} = -\frac{\beta I_{2*}^2}{(S_{2*}+I_{2*})^3}, \\
b_{11} &= \frac{2\beta S_{2*} I_{2*}}{(S_{2*}+I_{2*})^3}, \quad b_{02} = -\frac{\beta S_{2*}^2}{(S_{2*}+I_{2*})^3}, \\
a_{30} &= -\frac{\beta I_{2*}^2}{(S_{2*}+I_{2*})^4}, \quad a_{21} = \frac{\beta I_{2*}(2S_{2*}-I_{2*})}{3(S_{2*}+I_{2*})^4}, \\
a_{12} &= \frac{1}{3} \left(\frac{2\beta S_{2*}(2I_{2*}-S_{2*})}{3(S_{2*}+I_{2*})^4} + \frac{rk^2}{(1+kl_{2*})^3} \right), \quad a_{03} = \frac{1}{3} \left(\frac{\beta S_{2*}(2I_{2*}-S_{2*})}{(S_{2*}+I_{2*})^4} - \frac{3rk^3 S_{2*}}{(1+kl_{2*})^4} \right), \\
b_{30} &= \frac{\beta S_{2*} I_{2*}^2}{(S_{2*}+I_{2*})^4}, \quad b_{21} = \frac{\beta I_{2*}(I_{2*}-2S_{2*})}{3(S_{2*}+I_{2*})^4}, \\
b_{12} &= \frac{\beta S_{2*}(S_{2*}-2I_{2*})}{3(S_{2*}+I_{2*})^4}, \quad \text{and } b_{03} = \frac{\beta S_{2*}^2}{(S_{2*}+I_{2*})^4}.
\end{aligned}$$

Then, we expand the control parameter μ near the Turing bifurcation threshold as follows

$$\mu_T - \mu = \varepsilon \mu_1 + \varepsilon^2 \mu_2 + \varepsilon^3 \mu_3 + o(\varepsilon^3), \quad (44)$$

where $|\varepsilon| \ll 1$. Similar to Eq. (44), we expand the solution X , linear operator L and the nonlinear term \mathbf{H} into Taylor series at $\varepsilon = 0$.

$$X = \varepsilon \begin{pmatrix} U_1 \\ V_1 \end{pmatrix} + \varepsilon^2 \begin{pmatrix} U_2 \\ V_2 \end{pmatrix} + \varepsilon^3 \begin{pmatrix} U_3 \\ V_3 \end{pmatrix} + o(\varepsilon^3), \quad (45)$$

$$\mathbf{H} = \varepsilon^2 h_2 + \varepsilon^3 h_3 + o(\varepsilon^3), \quad (46)$$

$$L = L_T + (\mu_T - \mu)M, \quad (47)$$

where

$$h_2 = \begin{pmatrix} h_2^1 \\ h_2^2 \end{pmatrix} = \begin{pmatrix} a_{20}^T U_1^2 + a_{11}^T U_1 V_1 + a_{02}^T V_1^2 \\ b_{20}^T U_1^2 + b_{11}^T U_1 V_1 + b_{02}^T V_1^2 \end{pmatrix}, \quad (48)$$

and

$$\begin{aligned}
h_3 &= \begin{pmatrix} h_3^1 \\ h_3^2 \end{pmatrix} \\
&= \begin{pmatrix} a_{30}^T U^3 + a_{21}^T U^2 V + a_{12}^T U V^2 + a_{03}^T V^3 + 2(a_{20}^T U_1 U_2 + a_{02}^T V_1 V_2) + a_{11}^T (U_1 V_2 + V_1 U_2) \\ b_{30}^T U^3 + b_{21}^T U^2 V + b_{12}^T U V^2 + b_{03}^T V^3 + 2(b_{20}^T U_1 U_2 + b_{02}^T V_1 V_2) + b_{11}^T (U_1 V_2 + V_1 U_2) \end{pmatrix} \\
&\quad - \begin{pmatrix} \mu_1 (a_{20}' U_1^2 + a_{11}' U_1 V_1 + a_{02}' V_1^2) \\ \mu_1 (b_{20}' U_1^2 + b_{11}' U_1 V_1 + b_{02}' V_1^2) \end{pmatrix}, \quad (49)
\end{aligned}$$

with $a'_{ij} = \frac{da_{ij}}{d\mu}$, $b'_{ij} = \frac{db_{ij}}{d\mu}$, $(i, j = 0, 1, 2)$. Notice that the linear operator

$$L = L_T + (\mu_T - \mu)M, \quad (50)$$

where

$$L_T = \begin{pmatrix} a_{10} + d_1\Delta & a_{01} \\ b_{10} & b_{01} + d_2\Delta \end{pmatrix}_{\mu=\mu_T} \quad (51)$$

and

$$M = \begin{pmatrix} m_{11} & m_{12} \\ m_{21} & m_{22} \end{pmatrix} \quad (52)$$

with $m_{11} = \frac{da_{10}}{d\mu}$, $m_{12} = \frac{da_{01}}{d\mu}$, $m_{21} = \frac{db_{10}}{d\mu}$ and $m_{22} = \frac{db_{01}}{d\mu}$ at $U = S_{2*}$, $V = I_{2*}$.

Finally, the following multiple time scales are introduced

$$\frac{\partial}{\partial t} = \varepsilon \frac{\partial}{\partial T_1} + \varepsilon^2 \frac{\partial}{\partial T_2} + o(\varepsilon^2). \quad (53)$$

Substituting Eqs. (42)–(53) into Eq. (41) and expanding it with respect to different orders of ε^i , ($i = 1, 2, 3$),

$$\begin{aligned} \varepsilon : L_T \begin{pmatrix} U_1 \\ V_1 \end{pmatrix} &= 0, \\ \varepsilon^2 : L_T \begin{pmatrix} U_2 \\ V_2 \end{pmatrix} &= \frac{\partial}{\partial T_1} \begin{pmatrix} U_1 \\ V_1 \end{pmatrix} - \mu_1 M \begin{pmatrix} U_1 \\ V_1 \end{pmatrix} - h_2, \\ \varepsilon^3 : L_T \begin{pmatrix} U_3 \\ V_3 \end{pmatrix} &= \frac{\partial}{\partial T_1} \begin{pmatrix} U_2 \\ V_2 \end{pmatrix} + \frac{\partial}{\partial T_2} \begin{pmatrix} U_1 \\ V_1 \end{pmatrix} - \mu_1 M \begin{pmatrix} U_2 \\ V_2 \end{pmatrix} - \mu_2 M \begin{pmatrix} U_1 \\ V_1 \end{pmatrix} - h_3. \end{aligned} \quad (54)$$

Next, we find the amplitude equation by solving Eq. (54). Since L_T has an eigenvector associated with the zero eigenvalue $(f, 1)^T$ with $f = \frac{a_{10}d_2/d_1 - b_{01}}{2b_{10}}$. The general solution of the first component of Eq. (54) can be obtained

$$\begin{pmatrix} U_1 \\ V_1 \end{pmatrix} = \begin{pmatrix} f \\ 1 \end{pmatrix} \left(\sum_{j=1}^3 W_j e^{i\mathbf{k}_j \cdot \mathbf{r}} + c.c. \right), \quad (55)$$

where W_j is the amplitude of the mode $e^{i\mathbf{k}_j \cdot \mathbf{r}}$. The second component of Eq. (54) is nonhomogeneous, the adjoint operator of L_T is L_T^* , and it has the following zero eigenvectors form

$$\begin{pmatrix} 1 \\ g \end{pmatrix} e^{i\mathbf{k}_j \cdot \mathbf{r}} + c.c., \quad j = 1, 2, 3, \quad (56)$$

where $g = \frac{b_{01} - a_{10}d_2/d_1}{2b_{10}d_2/d_1}$. Let

$$\begin{pmatrix} F_U \\ F_V \end{pmatrix} = \frac{\partial}{\partial T_1} \begin{pmatrix} U_1 \\ V_1 \end{pmatrix} - \mu_1 \begin{pmatrix} m_{11}U_1 + m_{12}V_1 \\ m_{21}U_1 + m_{22}V_1 \end{pmatrix} - \begin{pmatrix} h_2^1 \\ h_2^2 \end{pmatrix}. \quad (57)$$

Then, with the help of Fredholm solvability condition

$$(1, g) \begin{pmatrix} F_U^j \\ F_V^j \end{pmatrix} = 0, \quad (58)$$

where F_U^j and F_V^j are the coefficients of $e^{i\mathbf{k}_j \cdot \mathbf{r}}$ in F_U and F_V , respectively. It follows after some routine calculation that for $j_l = 1, 2, 3$ and $j_l \neq l_m$ if $l \neq m$

$$(f + g) \frac{\partial W_{j1}}{\partial T_1} = \mu_1 h_3 W_{j1} - 2(h_1 + gh_2) \bar{W}_{j2} \bar{W}_{j3}, \quad (59)$$

where

$$h_1 = -(f^2 a_{20}^T + f a_{11}^T + a_{02}^T),$$

$$h_2 = -(f^2 b_{20}^T + f b_{11}^T + b_{02}^T),$$

$$h_3 = f m_{11} + m_{12} + g(f m_{21} + m_{22}).$$

Note that the forms of U_1 and V_1 are given by Eq. (55). We have a particular solution for the second component of Eq. (54) as follows:

$$\begin{aligned} \begin{pmatrix} U_2 \\ V_2 \end{pmatrix} &= \begin{pmatrix} \bar{U}_0 \\ \bar{V}_0 \end{pmatrix} + \sum_{j=1}^3 \begin{pmatrix} \bar{U}_j \\ \bar{V}_j \end{pmatrix} e^{i\mathbf{k}_j \cdot \mathbf{r}} + \sum_{j=1}^3 \begin{pmatrix} \bar{U}_{jj} \\ \bar{V}_{jj} \end{pmatrix} e^{i2\mathbf{k}_j \cdot \mathbf{r}} \\ &+ \begin{pmatrix} \bar{U}_{12} \\ \bar{V}_{12} \end{pmatrix} e^{i(\mathbf{k}_1 - \mathbf{k}_2) \cdot \mathbf{r}} + \begin{pmatrix} \bar{U}_{23} \\ \bar{V}_{23} \end{pmatrix} e^{i(\mathbf{k}_2 - \mathbf{k}_3) \cdot \mathbf{r}} \\ &+ \begin{pmatrix} \bar{U}_{31} \\ \bar{V}_{31} \end{pmatrix} e^{i(\mathbf{k}_3 - \mathbf{k}_1) \cdot \mathbf{r}} + c.c. \end{aligned} \quad (60)$$

with the coefficients given below at $\mu_T = \mu$

$$\begin{aligned} \begin{pmatrix} \bar{U}_0 \\ \bar{V}_0 \end{pmatrix} &= \begin{pmatrix} \frac{2(b_{01}h_1 - a_{01}h_2)}{\Delta_0} \\ \frac{2(a_{10}h_2 - b_{10}h_1)}{\Delta_0} \end{pmatrix} \sum_{j=1}^3 |W_j|^2 \\ &\equiv \begin{pmatrix} z_{U0} \\ z_{V0} \end{pmatrix} \sum_{j=1}^3 |W_j|^2, \bar{U}_j = f \bar{V}_j, \begin{pmatrix} X_{jj} \\ Y_{jj} \end{pmatrix} \equiv \begin{pmatrix} z_{U1} \\ z_{V1} \end{pmatrix} W_j^2 \\ &= \frac{1}{(a_{10} - 4d_1 j_{cr}^2)(b_{01} - 4d_2 j_{cr}^2) - a_{01}b_{10}} \times \begin{pmatrix} (b_{01} - 4d_2 j_{cr}^2)h_1 - a_{01}h_2 \\ (a_{10} - 4d_1 j_{cr}^2)h_2 - b_{10}h_1 \end{pmatrix} W_j^2 \end{aligned} \quad (61)$$

and

$$\begin{aligned} \begin{pmatrix} X_{jk} \\ Y_{jk} \end{pmatrix} &\equiv \begin{pmatrix} z_{U2} \\ z_{V2} \end{pmatrix} W_j \bar{W}_k \\ &= \frac{1}{(a_{10}-3d_1j_{cr}^2)(b_{01}-3d_2j_{cr}^2)-a_{01}b_{10}} \times \begin{pmatrix} (b_{01}-3d_2j_{cr}^2)h_1-a_{01}h_2 \\ (a_{10}-3d_1j_{cr}^2)h_2-b_{10}h_1 \end{pmatrix} W_j \bar{W}_k. \end{aligned} \quad (62)$$

For the third component of Eq. (54), we apply Fredholm solvability condition again, and get for $j = 1$

$$\begin{aligned} (f+g) \left(\frac{\partial V_j}{\partial T_1} + \frac{\partial W_j}{\partial T_2} \right) &= h_3(\mu_1 V_j + \mu_2 W_j) + h_4 \bar{W}_l \bar{W}_m + H(\bar{V}_l \bar{W}_m + \bar{V}_m \bar{W}_l) \\ &\quad - (G_1 |W_1|^2 + G_2 (|W_2|^2 + |W_3|^2)) W_j \end{aligned} \quad (63)$$

with

$$h_4 = -2\mu_1(a_{20}'f^2 + a_{11}'f + a_{02}' + g(b_{20}'f^2 + a_{11}'f + b_{02}')), \quad (64)$$

$$H = -2(h_1 + gh_2), \quad (65)$$

$$\begin{aligned} G_1 &= -(3a_{30}f^3 + 2a_{11}fz_{V0} + a_{11}fz_{V1} + 4a_{20}fz_{U0} + 2a_{20}fz_{U1} \\ &\quad + 3a_{21}f^2 + 4a_{02}z_{V0} + 2a_{02}z_{V1} + 2a_{11}z_{U0} \\ &\quad + a_{11}z_{U1} + 3a_{12}f + 3a_{03}) \\ &\quad - g(b_{30}f^3 + 2b_{11}fz_{V0} + b_{11}fz_{V1} + 4b_{20}fz_{U0} + 2b_{20}fz_{U1} \\ &\quad + 3b_{21}f^2 + 4b_{02}z_{V0} + 2b_{02}z_{V1} + 2b_{11}z_{U0} \\ &\quad + b_{11}z_{U1} + 3b_{12}f + 3b_{03}), \end{aligned} \quad (66)$$

and

$$\begin{aligned} G_2 &= -(6a_{30}f^3 + 2a_{11}fz_{V0} + a_{11}fz_{V2} + 4a_{20}fz_{U0} + 2a_{20}fz_{U2} \\ &\quad + 6a_{21}f^2 + 4a_{02}z_{V0} + 2a_{02}z_{V2} + 2a_{11}z_{U0} \\ &\quad + a_{11}z_{U2} + 6a_{12}f + 6a_{03}) \\ &\quad - g(6b_{30}f^3 + 2b_{11}fz_{V0} + b_{11}fz_{V2} + 4b_{20}fz_{U0} + 2b_{20}fz_{U2} \\ &\quad + 6b_{21}f^2 + 4b_{02}z_{V0} + 2b_{02}z_{V2} + 2b_{11}z_{U0} \\ &\quad + b_{11}z_{U2} + 6b_{12}f + 6b_{03}). \end{aligned} \quad (67)$$

The amplitude equation Eq. (68) of amplitude A_j is given as follows, by combining Eq. (59) with Eq. (63)

$$\tau_0 \frac{\partial A_j}{\partial t} = \mu A_j + h \bar{A}_l \bar{A}_m - (g_1 |A_1|^2 + g_2 (|A_2|^2 + |A_3|^2)) A_j \quad (68)$$

where

$$\tau_0 = \frac{f + g}{\mu_T [fm_{11} + m_{12} + g(fm_{21} + m_{22})]}, \quad (69)$$

$$\sigma = \frac{\mu_T - \mu}{\mu_T}, \quad (70)$$

$$h = \frac{H}{\mu_T [fm_{11} + m_{12} + g(fm_{21} + m_{22})]}, \quad (71)$$

$$g_i = \frac{G_i}{\mu_T [fm_{11} + m_{12} + g(fm_{21} + m_{22})]}. \quad (72)$$

It is worth noting that Eq. (68) is in complex form. According to the method of reference³⁵, for the convenience of discussion, we convert it into real form with the help of $A_j = \rho_j \exp(i\varphi_j)$, as follow:

$$\begin{cases} \tau_0 \frac{\partial \varphi}{\partial t} = -h \frac{\rho_1^2 \rho_2^2 + \rho_1^2 \rho_3^2 + \rho_2^2 \rho_3^2}{\rho_1 \rho_2 \rho_3} \sin \varphi, \\ \tau_0 \frac{\partial \rho_1}{\partial t} = \sigma \rho_1 + h \rho_2 \rho_3 \cos \varphi - g_1 \rho_1^3 - g_2 (\rho_3^2 + \rho_2^2) \rho_1, \\ \tau_0 \frac{\partial \rho_2}{\partial t} = \sigma \rho_2 + h \rho_1 \rho_3 \cos \varphi - g_1 \rho_2^3 - g_2 (\rho_3^2 + \rho_1^2) \rho_2, \\ \tau_0 \frac{\partial \rho_3}{\partial t} = \sigma \rho_3 + h \rho_2 \rho_1 \cos \varphi - g_1 \rho_3^3 - g_2 (\rho_1^2 + \rho_2^2) \rho_3, \end{cases} \quad (73)$$

where ρ_j are the real amplitudes and φ_j are the phase angles, and $\varphi = \varphi_1 + \varphi_2 + \varphi_3$. Since we only focus on the stable steady state and notice the fact that $h\rho_i \neq 0$, according to first equation of (73), we obtain $\varphi = 0$ or π . In addition, we know that $\tau_0 > 0$, which means that when $h > 0$, the state corresponding to $\varphi = 0$ is stable, while when $h < 0$, the state corresponding to $\varphi = \pi$ is stable. After that, model of amplitude equations (73) becomes

$$\begin{cases} \tau_0 \frac{\partial \rho_1}{\partial t} = \sigma \rho_1 + |h| \rho_2 \rho_3 - g_1 \rho_1^3 - g_2 (\rho_3^2 + \rho_2^2) \rho_1, \\ \tau_0 \frac{\partial \rho_2}{\partial t} = \sigma \rho_2 + |h| \rho_1 \rho_3 - g_1 \rho_2^3 - g_2 (\rho_3^2 + \rho_1^2) \rho_2, \\ \tau_0 \frac{\partial \rho_3}{\partial t} = \sigma \rho_3 + |h| \rho_2 \rho_1 - g_1 \rho_3^3 - g_2 (\rho_1^2 + \rho_2^2) \rho_3. \end{cases} \quad (74)$$

The amplitude equations are usually valid only when the control parameter μ is in Turing space. It is not difficult to see that the above ordinary differential equations (74) have five equilibrium points, corresponding to five steady states^{20,29,30,33–36}. Considering the symmetry of the model, we have

- Model (74) always makes an equilibrium $E_0 = (0, 0, 0)$ is stable for $\sigma < \sigma_2 = 0$ and unstable for $\sigma > \sigma_2$.
- Model (74) has an equilibrium $E_s = (\sqrt{\frac{\sigma}{g_1}}, 0, 0)$ corresponding to stripe patterns, which is stable for $\mu > \sigma_3 = \frac{h^2 g_1}{(g_2 - g_1)^2}$ and unstable for $\sigma > \sigma_3$.

- Model (74) has an equilibrium $E_h = (\rho_h^{1\pm}, \rho_h^{2\pm}, \rho_h^{3\pm})$ corresponding to hexagon patterns, with $\varphi = 0$ or $\varphi = \pi$, and $\rho_h^{(1,2,3)+} = \frac{|h| + \sqrt{h^2 + 4(g_1 + 2g_2)\sigma}}{2(g_1 + 2g_2)}$ is stable for $\sigma < \sigma_4 = \frac{h^2(2g_1 + g_2)}{(g_2 - g_1)^2}$, $\rho_h^{(1,2,3)-} = \frac{|h| - \sqrt{h^2 + 4(g_1 + 2g_2)\sigma}}{2(g_1 + 2g_2)}$ is unstable. Where

$$\rho_h^{1\pm} = \rho_h^{2\pm} = \rho_h^{3\pm} = \frac{|h| \pm \sqrt{h^2 + 4(g_1 + 2g_2)\sigma}}{2(g_1 + 2g_2)}.$$

- Model (74) has an equilibrium $E_m = (\rho_m^1, \rho_m^2, \rho_m^3)$ corresponding to mixed patterns, with $g_1 > g_2$, $\sigma > g_1\rho_1^2$ and which is unstable. Where

$$\rho_m^1 = \frac{|h|}{g_2 - g_1}, \rho_m^2 = \rho_m^3 = \sqrt{\frac{\sigma - g_1\rho_1^2}{g_2 + g_1}}.$$

IV. NUMERICAL SIMULATIONS

In this section, we simulate the spatial model (2) by using the two-dimensional positive bounded domain $\Omega \subseteq \mathbb{R}_+^2$ with the initial condition of a positive random number between 0 and 1 with zero-flux boundary. We discretize the time and space, respectively, and distribute the space in the grid of $L_x = L_y = 20$, where the space step is $\Delta h = 0.2$, and the time step is $\Delta t = 0.01$. The reaction terms are discretized by Euler scheme. The standard five-point explicit finite difference scheme is adopted for the Laplace operator (i.e., diffusion term)^{10,20,31,34,37}, as follows:

$$\Delta_h S_{i,j}^n = \frac{S_{i+1,j}^n + S_{i-1,j}^n + S_{i,j+1}^n + S_{i,j-1}^n - 4S_{i,j}^n}{\Delta h^2}, \quad (75)$$

$$\Delta_h I_{i,j}^n = \frac{I_{i+1,j}^n + I_{i-1,j}^n + I_{i,j+1}^n + I_{i,j-1}^n - 4I_{i,j}^n}{\Delta h^2}. \quad (76)$$

The parameter values are shown in Table II.

A. Pattern formation by death rate

In the numerical simulation, we found different shapes of patterns, and found that the distributions of uninfected host S and infected host I are always the same type. We, therefore, only consider the distribution of uninfected hosts S for the sake of brevity. The main factors affecting Turing instability were death rate, fear effect, reducing reproduction ability of infected hosts and diffusion coefficient. Therefore, the idea of our numerical experiment is to consider the influence of different

TABLE II. Description of parameters and their fixed values for model (2).

| Parameter | Description | Value |
|-----------|---|------------------|
| r | maximum birth rate of the hosts | 0.60^{10} |
| k | level of fear which drives anti-infected host behavior of uninfected host | control variable |
| ρ | reducing reproduction ability of infected hosts | control variable |
| $1/a$ | carrying capacity | $1^{2,10}$ |
| β | disease transmission rate | $1^{2,10}$ |
| μ | death rate of the infected host population | control variable |
| d_1 | diffusion coefficients of S | control variable |
| d_2 | diffusion coefficients of I | control variable |

parameters on the root of the characteristic equation (32), and to simulate the population distribution under each parameter, that is, pattern formation. First, we plan to simulate the effects of different mortality rates on population distribution. From Fig. 2 and Fig. 3, we set the diffusion coefficients of S and I are $d_1 = 0.01$ and $d_2 = 0.25^{10}$, natural death rate μ to $\mu = 0.4, \mu = 0.51, \mu = 0.54, \mu = 0.55, \mu = 0.56$ and $\mu = 0.57$, other parameters are $k = 0.4, \rho = 0.1^{10}$ and shown in Table II. The corresponding positive equilibrium are $E_{2*} = (0.0434, 0.0650), E_{2*} = (0.1110, 0.1066), E_{2*} = (0.1364, 0.1162), E_{2*} = (0.1456, 0.1191), E_{2*} = (0.1551, 0.1219), E_{2*} = (0.1650, 0.1245)$. Fig. 2 shows that maximum real part of the roots of Eq. (32) and $\text{Det}(J_{n*}^j)$ against j for different μ taken from the Turing region, respectively. we observe the change of the pattern shape, as presented in Fig. 3. The results show that natural death rate can control the growth of pattern, following: hot spots (Fig. 3(a)) \rightarrow hot spots-stripes (Fig. 3(b)) \rightarrow hot stripes (Fig. 3(c)) \rightarrow cold stripes (Fig. 3(d)) \rightarrow cold spots-stripes (Fig. 3(e)) \rightarrow cold spots (Fig. 3(f)).

B. Pattern formation by fear effect

In this subsection, we plan to observe the distribution of the population under different degrees of fear. From Fig. 4 and Fig. 5, we set the diffusion coefficients of S and I are $d_1 = 0.01$ and $d_2 = 0.25^{10}$, fear effect k to $k = 0.01, k = 0.25, k = 0.42, k = 0.5, k = 1.8$ and $k = 3$, other parameters are $\mu = 0.55, \rho = 0.1^{10}$ and shown in Table II. The corresponding positive equilibrium are $E_{2*} = (0.1680, 0.1375), E_{2*} = (0.1532, 0.1254), E_{2*} = (0.1446, 0.1183), E_{2*} = (0.1410, 0.1153), E_{2*} =$

Pattern formation of parasite-host model induced by fear effect

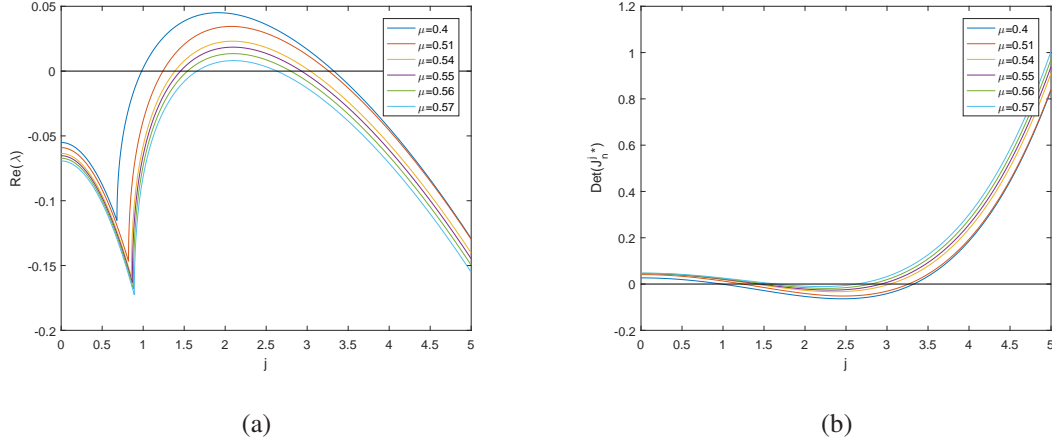


FIG. 2. Plots of (a) the maximum real part of the roots of Eq. (32) and (b) $\text{Det}(J_{n*}^j)$ against j for different μ taken from the Turing region. Other parameters are set to $d_1 = 0.01$, $d_2 = 0.25$, $\rho = 0.1$ and $k = 0.4$.

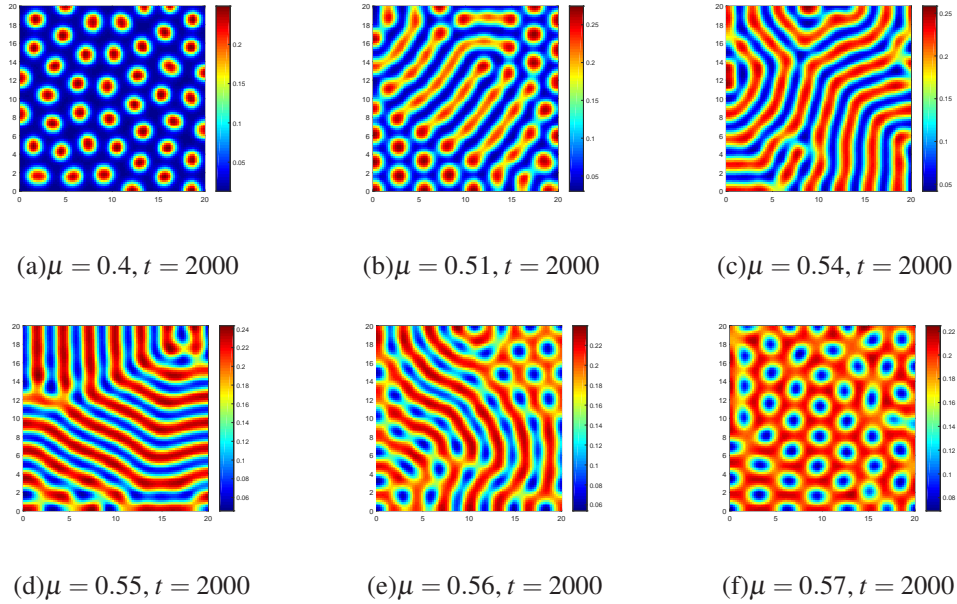


FIG. 3. Natural death rate of infected hosts: (a) $\mu = 0.4$, (b) $\mu = 0.51$, (c) $\mu = 0.54$, (d) $\mu = 0.55$, (e) $\mu = 0.56$, (f) $\mu = 0.57$. Natural death rate control the growth of pattern, following: hot spots \rightarrow hot spots-strips \rightarrow hot strips \rightarrow cold strips \rightarrow cold spots-strips \rightarrow cold spots for $d_1 = 0.01$, $d_2 = 0.25$, $\rho = 0.1$ and $k = 0.4$.

$(0.1022, 0.0836)$, $E_{2*} = (0.0828, 0.0678)$. Fig. 4 shows that maximum real part of the roots of Eq. (32) and $\text{Det}(J_{n*}^j)$ against j for different k taken from the Turing region. Respectively, we observed the change of the pattern shape. The results showed that fear effect can control the growth of pattern: cold spots (Fig. 5(a)) \rightarrow cold spots-strips (Fig. 5(b)) \rightarrow cold strips (Fig. 5(c))

Pattern formation of parasite-host model induced by fear effect

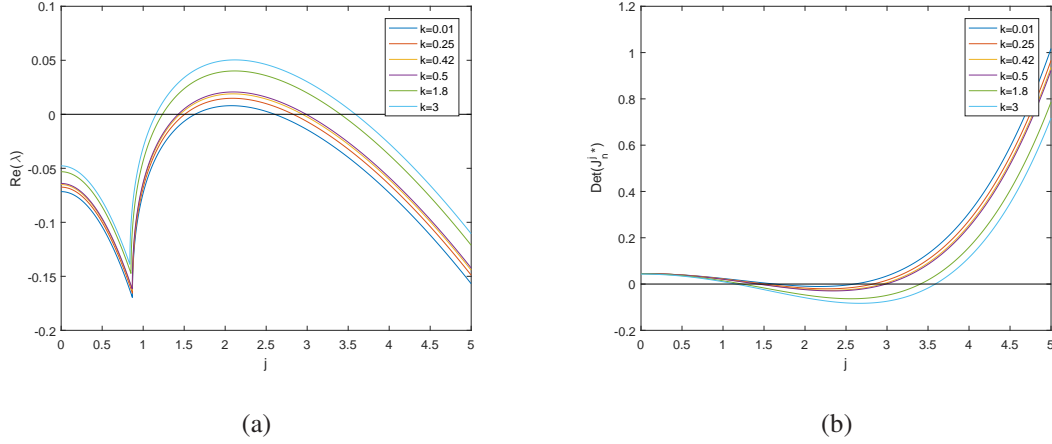


FIG. 4. Plots of (a) the maximum real part of the roots of Eq. (32) and (b) $\text{Det}(J_{n*}^j)$ against j for different k taken from the Turing region. Other parameters are set to $d_1 = 0.01$, $d_2 = 0.25$, $\rho = 0.1$ and $\mu = 0.55^{10}$.

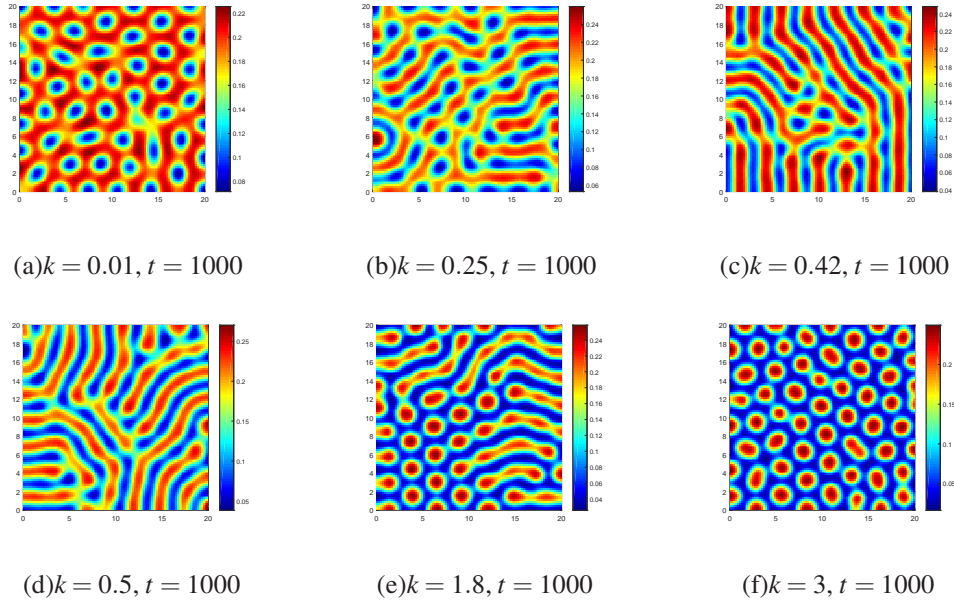


FIG. 5. Fear effect: (a) $k = 0.01$, (b) $k = 0.25$, (c) $k = 0.42$, (d) $k = 0.5$, (e) $k = 1.8$, (f) $k = 3$. Fear effect controls the growth of pattern: Cold spots \rightarrow cold spots-strips \rightarrow cold stripes \rightarrow hot stripes \rightarrow hot spots-strips \rightarrow hot spots for $d_1 = 0.01$, $d_2 = 0.25$, $\rho = 0.1$ and $\mu = 0.55$.

\rightarrow hot stripes (Fig. 5(d)) \rightarrow hot spots-strips (Fig. 5(e)) \rightarrow hot spots (Fig. 5(f)).

Pattern formation of parasite-host model induced by fear effect

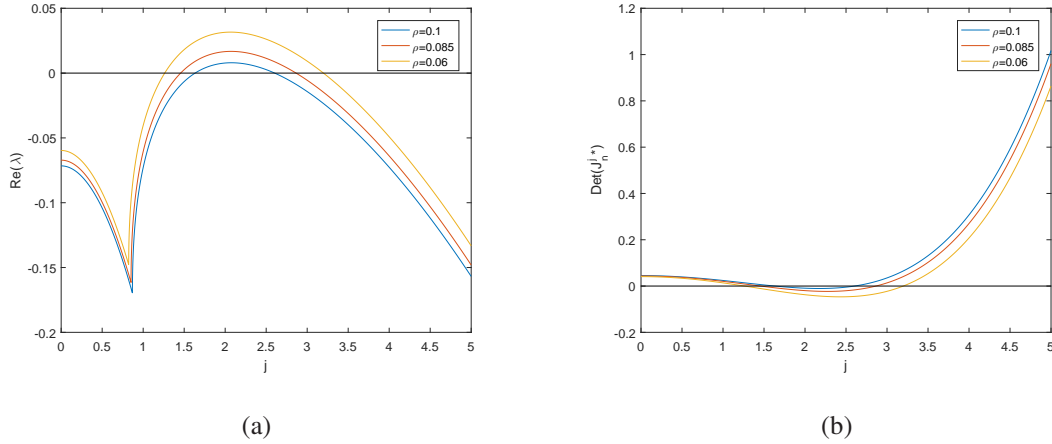


FIG. 6. Plots of (a) the maximum real part of the roots of Eq. (32) and (b) $Det(J_{n*}^j)$ against j for different ρ taken from the Turing region. Other parameters are set to $d_1 = 0.01$, $d_2 = 0.25$, $\mu = 0.55$ and $k = 0.01$.

C. Pattern formation by reducing reproduction ability of infected hosts

Then, we plan to observe the effect of reducing reproduction ability of infected hosts on population distribution. From Fig. 6 and Fig. 7, we set the fear effect is $k = 0.01$, diffusion coefficients of S is $d_1 = 0.01$ ¹⁰, diffusion coefficients of I is $d_2 = 0.25$ ¹⁰ and reducing reproduction ability of infected hosts $\rho = 0.085$ and $\rho = 0.06$, other parameters are $\mu = 0.55$ ¹⁰ and shown in Table II. Fig. 6 shows that maximum real part of the roots of Eq. (32) and $Det(J_{n*}^j)$ against j for different ρ taken from the Turing region. Respectively, we observed the change of the pattern shape. The results showed that reducing reproduction ability of infected hosts can control the growth of pattern: cold spots-stripes pattern (Fig. 7(a)) \rightarrow cold stripes pattern (Fig. 7(b)).

D. Pattern formation by diffusion

Finally, we give the influence of the self diffusion coefficients of the susceptible and infected on the population distribution. From Fig. 8 and Fig. 9, we set the fear effect is $k = 0.01$, reducing reproduction ability of infected hosts $\rho = 0.1$ ¹⁰, diffusion coefficients of S is $d_1 = 0.01$ ¹⁰ and diffusion coefficients of I to $d_2 = 0.32$ and $d_2 = 3$, other parameters are $\mu = 0.55$ ¹⁰ and shown in Table II. Fig. 8 shows that maximum real part of the roots of Eq. (32) and $Det(J_{n*}^j)$ against j for different d_2 taken from the Turing region. Respectively, we observed the change of the pattern shape. The results showed that self diffusion coefficient of the susceptible can control the growth

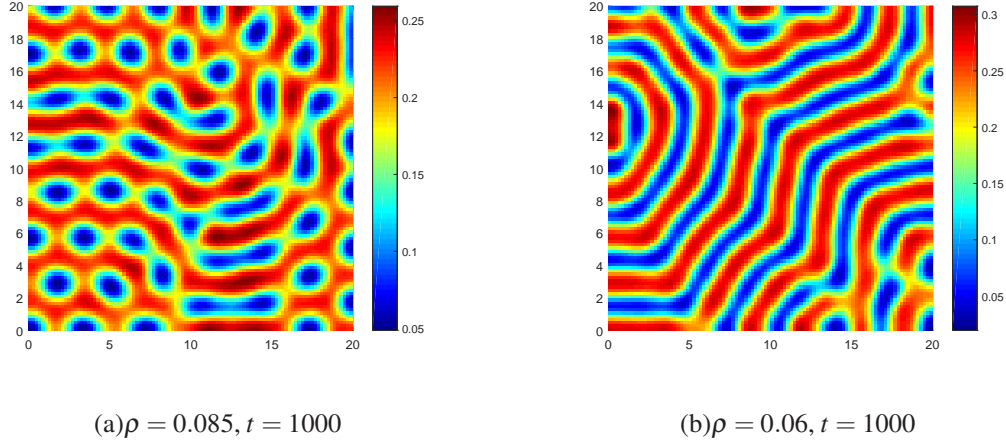


FIG. 7. Reducing reproduction ability of infected hosts: (a) $\rho = 0.085$, (b) $\rho = 0.06$. Reducing reproduction ability of infected hosts controls the growth of pattern: cold spots-strips, stripes pattern formation for $d_1 = 0.01$, $d_2 = 0.25$, $\mu = 0.55$ and $k = 0.01$.

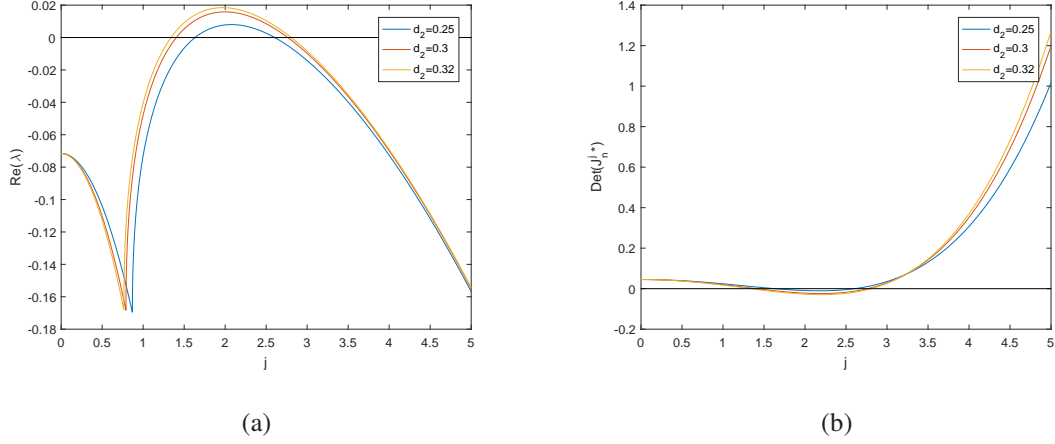


FIG. 8. Plots of (a) the maximum real part of the roots of Eq. (32) and (b) $\text{Det}(J_{n*}^j)$ against j for different d_2 taken from the Turing region. Other parameters are set to $d_1 = 0.01$, $k = 0.01$, $\rho = 0.1$ and $\mu = 0.55$.

of pattern: cold spots-strips pattern (Fig. 9(a)) \rightarrow cold stripes pattern. (Fig. 9(b)).

From Fig. 10 and Fig. 11, we set the fear effect is $k = 0.01$, reducing reproduction ability of infected hosts $\rho = 0.1$ ¹⁰, diffusion coefficients of I is $d_2 = 0.25$ ¹⁰ and diffusion coefficients of S to $d_1 = 0.008$ and $d_1 = 0.005$, other parameters are $\mu = 0.55$ ¹⁰ and shown in Table II. Fig. 10 shows that maximum real part of the roots of Eq. (32) and $\text{Det}(J_{n*}^j)$ against j for different d_1 taken from the Turing region. Respectively, we observed the change of the pattern shape. The results showed that self diffusion coefficient of the infected can control the growth of pattern: cold spots-strips pattern (Fig. 11(a)) \rightarrow cold stripes pattern (Fig. 11(b)).

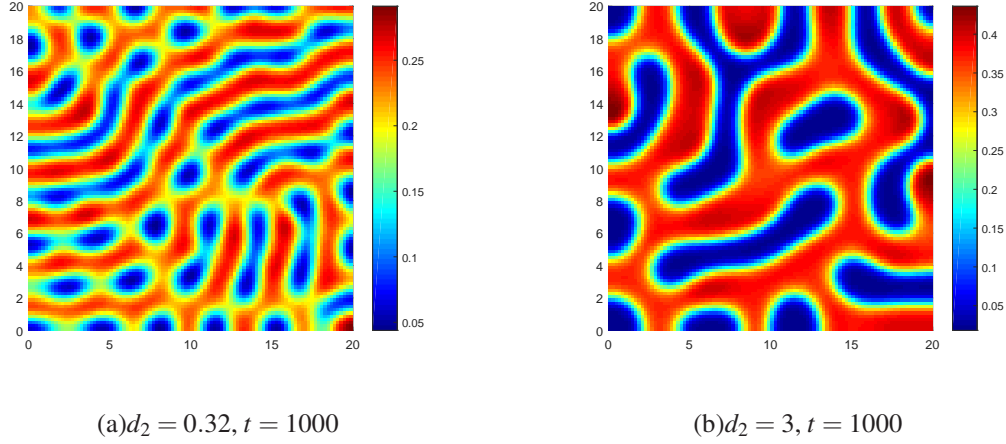


FIG. 9. Diffusion coefficient: (a) $d_2 = 0.32$, (b) $d_2 = 3$. Self diffusion coefficient of the susceptible controls the growth of pattern: cold spots-stripes, stripes pattern formation for $d_1 = 0.01$, $k = 0.01$, $\rho = 0.1$ and $\mu = 0.55$.

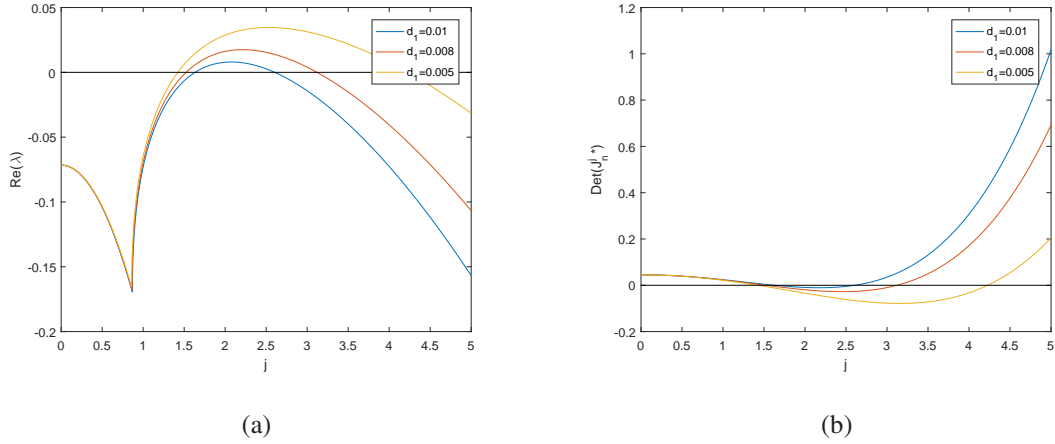


FIG. 10. Plots of (a) the maximum real part of the roots of Eq. (32) and (b) $\text{Det}(J_{n*}^j)$ against j for different d_1 taken from the Turing region. Other parameters are set to $d_2 = 0.25$, $k = 0.01$, $\rho = 0.1$ and $\mu = 0.55$.

V. CONCLUSIONS

In conclusion, we study the pattern formation of a host parasite model induced by fear effect. The conditions of Turing instability are obtained through theoretical analysis. With the help of numerical simulation, the influence of various parameters on the pattern formation is explored by selecting different control parameters (natural mortality μ , fear effect k , reducing reproduction ability ρ , diffusion coefficient d_1, d_2). Through the observation of the pattern growth, we find some interesting phenomena. The results show that under the effect of fear, the pattern growth

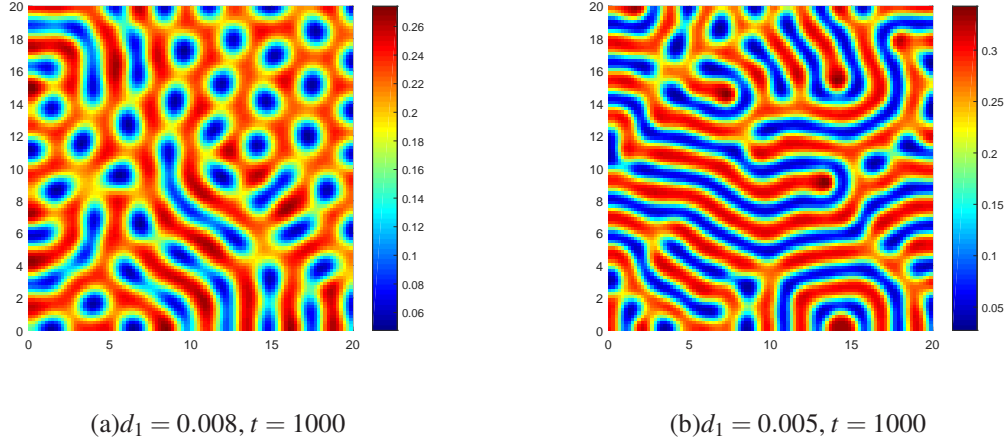


FIG. 11. Diffusion coefficient: (a) $d_1 = 0.008$, (b) $d_1 = 0.005$. Self diffusion coefficient of the infected controls the growth of pattern: cold spots-strips, stripes pattern formation for $d_2 = 0.25$, $k = 0.01$, $\rho = 0.1$ and $\mu = 0.55$.

mechanism is always unified, growing in the form of cold spots \rightarrow cold spots-strips \rightarrow cold strips \rightarrow hot strips \rightarrow hot spots-strips \rightarrow hot spots, which is also consistent with the results of literature¹⁷. Moreover, we also find that the change of pattern growth caused by natural mortality was opposite to that of fear factor.

The dynamic phenomena of ODE predator-prey system considering fear effect include: promoting stability, periodic solution (limit cycle), making chaotic state become stable and so on^{1,14,16,18,19,21–26}. However, researches on the change of spatial population dynamics caused by fear effect are still not general. Through the description of^{17,27}, we can find that the evolution of pattern induced by fear effect often follows the rule that with the increase of fear, the growth order of pattern is: cold spots \rightarrow cold spots-strips \rightarrow cold strips \rightarrow hot strips \rightarrow hot spots-strips \rightarrow hot spots. As for whether such a conclusion is general, we need to continue to explore in our future work.

ACKNOWLEDGMENTS

This work was supported by the Innovative Research Project of Shenzhen under Project No. KQJSCX20180328165509766, Nature Science Foundation of Guangdong Province under Project No. 2020A1515010812 and 2021A1515011594.

DATA AVAILABILITY

Data sharing is not applicable to this article as no new data were created or analyzed in this study.

REFERENCES

- ¹X. Wang, L. Zanette, and X. Zou, “Modelling the fear effect in predator–prey interactions,” *Journal of mathematical biology* **73**, 1179–1204 (2016).
- ²T.-W. Hwang and Y. Kuang, “Deterministic extinction effect of parasites on host populations,” *Journal of mathematical biology* **46**, 17–30 (2003).
- ³D. Ebert, M. Lipsitch, and K. L. Mangin, “The effect of parasites on host population density and extinction: experimental epidemiology with daphnia and six microparasites,” *The American Naturalist* **156**, 459–477 (2000).
- ⁴H. W. Hethcote, “The mathematics of infectious diseases,” *SIAM review* **42**, 599–653 (2000).
- ⁵T.-W. Hwang and Y. Kuang, “Host extinction dynamics in a simple parasite-host interaction model,” *Mathematical Biosciences & Engineering* **2**, 743 (2005).
- ⁶E. E. Holmes, M. A. Lewis, J. Banks, and R. Veit, “Partial differential equations in ecology: spatial interactions and population dynamics,” *Ecology* **75**, 17–29 (1994).
- ⁷C. Neuhauser, “Mathematical challenges in spatial ecology,” *Notices of the AMS* **48**, 1304–1314 (2001).
- ⁸A. Okubo and S. A. Levin, *Diffusion and ecological problems: modern perspectives*, Vol. 14 (Springer, 2001).
- ⁹W. Wang, X. Gao, Y. Cai, H. Shi, and S. Fu, “Turing patterns in a diffusive epidemic model with saturated infection force,” *Journal of the Franklin Institute* **355**, 7226–7245 (2018).
- ¹⁰B. Zhang, Y. Cai, B. Wang, and W. Wang, “Pattern formation in a reaction–diffusion parasite–host model,” *Physica A: Statistical Mechanics and its Applications* **525**, 732–740 (2019).
- ¹¹Y. Cai and W. Wang, “Dynamics of a parasite-host epidemiological model in spatial heterogeneous environment,” *Discrete & Continuous Dynamical Systems-B* **20**, 989 (2015).
- ¹²L. Y. Zanette, A. F. White, M. C. Allen, and M. Clinchy, “Perceived predation risk reduces the number of offspring songbirds produce per year,” *Science* **334**, 1398–1401 (2011).

- ¹³R. N. Abbey-Lee, K. J. Mathot, and N. J. Dingemanse, “Behavioral and morphological responses to perceived predation risk: a field experiment in passerines,” *Behavioral Ecology* **27**, 857–864 (2016).
- ¹⁴P. Panday, N. Pal, S. Samanta, and J. Chattopadhyay, “A three species food chain model with fear induced trophic cascade,” *International Journal of Applied and Computational Mathematics* **5**, 1–26 (2019).
- ¹⁵M. Mandal, S. Jana, S. K. Nandi, and T. K. Kar, “Modelling and control of a fractional-order epidemic model with fear effect,” *Energy, ecology & environment*, 1–12 (2020).
- ¹⁶S. K. Sasmal and Y. Takeuchi, “Dynamics of a predator-prey system with fear and group defense,” *Journal of Mathematical Analysis and Applications* **481**, 123471 (2020).
- ¹⁷B. Chakraborty, H. Baek, and N. Bairagi, “Diffusion-induced regular and chaotic patterns in a ratio-dependent predator–prey model with fear factor and prey refuge,” *Chaos: An Interdisciplinary Journal of Nonlinear Science* **31**, 033128 (2021).
- ¹⁸J. Wang, Y. Cai, S. Fu, and W. Wang, “The effect of the fear factor on the dynamics of a predator-prey model incorporating the prey refuge,” *Chaos: An Interdisciplinary Journal of Nonlinear Science* **29**, 083109 (2019).
- ¹⁹X. Wang, Y. Tan, Y. Cai, and W. Wang, “Impact of the fear effect on the stability and bifurcation of a leslie–gower predator–prey model,” *International Journal of Bifurcation and Chaos* **30**, 2050210 (2020).
- ²⁰M. Francesca Carfora and I. Torcicollo, “Cross-diffusion-driven instability in a predator-prey system with fear and group defense,” *Mathematics* **8**, 1244 (2020).
- ²¹P. Panday, N. Pal, S. Samanta, and J. Chattopadhyay, “Stability and bifurcation analysis of a three-species food chain model with fear,” *International Journal of Bifurcation and Chaos* **28**, 1850009 (2018).
- ²²P. Cong, M. Fan, and X. Zou, “Dynamics of a three-species food chain model with fear effect,” *Communications in Nonlinear Science and Numerical Simulation* **99**, 105809 (2021).
- ²³T. Qiao, Y. Cai, S. Fu, and W. Wang, “Stability and hopf bifurcation in a predator-prey model with the cost of anti-predator behaviors,” *International Journal of Bifurcation and Chaos* **29** (2019).
- ²⁴S. K. Sasmal, “Population dynamics with multiple allee effects induced by fear factors - a mathematical study on prey-predator interactions,” *Applied Mathematical Modelling* **64**, 1–14 (2018).
- ²⁵X. Wang and X. Zou, “Modeling the fear effect in predator-prey interactions with adaptive avoidance of predators,” *Bulletin of Mathematical Biology* **79**, 1325–1359 (2017).
- ²⁶H. Zhang, Y. Cai, S. Fu, and W. Wang, “Impact of the fear effect in a prey-predator model incorporating a prey refuge,” *Applied Mathematics and Computation* **356**, 328–337 (2019).

- ²⁷R. Han, L. N. Guin, and B. Dai, “Cross-diffusion-driven pattern formation and selection in a modified leslie-gower predator-prey model with fear effect,” *Journal of Biological Systems* **28**, 27–64 (2020).
- ²⁸Y. Ye and Y. Zhao, “Bifurcation analysis of a delay-induced predator-prey model with allee effect and prey group defense,” *International Journal of Bifurcation and Chaos* **31**, 2150158 (2021).
- ²⁹T. Zhang, Y. Xing, H. Zang, and M. Han, “Spatio-temporal dynamics of a reaction-diffusion system for a predator–prey model with hyperbolic mortality,” *Nonlinear Dynamics* **78**, 265–277 (2014).
- ³⁰D. Jana, S. Batabyal, and M. Lakshmanan, “Self-diffusion-driven pattern formation in prey-predator system with complex habitat under fear effect,” *The European Physical Journal Plus* **135** (2020).
- ³¹F. Capone, M. F. Carfora, R. De Luca, and I. Torricollo, “Turing patterns in a reaction-diffusion system modeling hunting cooperation,” *Mathematics and Computers in Simulation* **165**, 172–180 (2019).
- ³²M. Ipsen, F. Hynne, and P. Sørensen, “Amplitude equations for reaction–diffusion systems with a hopf bifurcation and slow real modes,” *Physica D: Nonlinear Phenomena* **136**, 66–92 (2000).
- ³³S. Yuan, C. Xu, and T. Zhang, “Spatial dynamics in a predator-prey model with herd behavior,” *Chaos: An Interdisciplinary Journal of Nonlinear Science* **23**, 033102 (2013).
- ³⁴W. Wei-Ming, W. Wen-Juan, L. Ye-Zhi, and T. Yong-Ji, “Pattern selection in a predation model with self and cross diffusion,” *Chinese Physics B* **20**, 034702 (2011).
- ³⁵Q. Ouyang, “Nonlinear science and the pattern dynamics introduction,” (2010).
- ³⁶H. Liu, Y. Ye, Y. Wei, W. Ma, M. Ma, and K. Zhang, “Pattern formation in a reaction-diffusion predator-prey model with weak allee effect and delay,” *Complexity* **2019** (2019).
- ³⁷M. R. Garvie, “Finite-difference schemes for reaction-diffusion equations modeling predator-prey interactions in matlab,” *Bulletin of Mathematical Biology* **69**, 931–956 (2007).